DOI 10.1007/s10946-021-09997-8
Journal of Russian Laser Research, Volume 42, Number 5, September, 2021

TERAHERTZ DUAL-BAND NEAR-ZERO EFFECTIVE INDEX METAMATERIAL BASED ON DOUBLE-SIDED METAL MICROSTRUCTURE

Tianqi Zhao,[1] Tianzi Luo,[1] Bo Fang,[2] Lijiang Shi,[3] Yongxing Jin,[1*] Pengwei Zhou,[1,4] Dong Yao,[4] Chenxia Li,[1] Xufeng Jing,[1,5] and Zhi Hong[5]

[1] *Institute of Optoelectronic Technology, China Jiliang University Hangzhou 310018, China*

[2] *College of Metrology and Measurement Engineering, China Jiliang University Hangzhou 310018, China*

[3] *Hangzhou Hangxin Qihui Technology Co. Ltd Hangzhou 310018, China*

[4] *Key Laboratory of Airborne Optical Imaging and Measurement Changchun Institute of Optics, Fine Mechanics and Physics, Chinese Academy of Science Changchun 130033, China*

[5] *Centre for THz Research, China Jiliang University Hangzhou 310018, China*

*Corresponding author e-mail: jinyongxing @ cjlu.edu.cn

Abstract

The zero-refractive-index metamaterials have excellent electromagnetic properties, which provide new ideas and methods to realize the control of electromagnetic waves and the design of new photoelectric devices. Here, we propose a double-sided metamaterial structure to achieve double-zero refractive index in the terahertz region. We use the S parameter inversion algorithm to extract the equivalent electromagnetic parameters of the metamaterial. By optimizing the design of structural parameters, we show that the effective refractive index can be achieved to be near zero at 0.5 – 1.7 THz and at 2.7 – 3.4 THz. By monitoring the current density distribution and the near-field distribution on the surface of the structure, we prove that the metamaterial structure has obvious zero refractive index effect at 1.66 and 3.34 THz. In addition, the influence of geometric parameters of metamaterial structures on equivalent refractive index is revealed.

Keywords: metamaterial, zero refractive index, terahertz wave.

1. Introduction

Metamaterials are a kind of microstructures composed of periodic or aperiodic subwavelength units that exhibit novel electromagnetic properties not found in the nature [1–15]. Metamaterials provide an effective way to achieve free control of electromagnetic waves [16–30]. As a special metamaterial, the zero-index metamaterial (ZIM) has attracted much attention in recent years due to its unique characteristic, in which the quasi-infinite wavelength and phase velocity are revealed. This unique phase characteristic provides high flexibility in the manipulation of electromagnetic wave propagation, absorption, and

Manuscript submitted by the authors in English on April 7, 2021.

polarization. Many research results on ZIMs have been successfully applied to the fields of ideal lenses and highly-directional antennas [31, 32]. Due to their excellent electromagnetic properties, ZIMs provide new ideas and methods for realizing control of electromagnetic waves and the design of photoelectric devices. Researchers have successfully developed various functional devices with ZIMs such as waveform converters, superlens, field rotator, invisibility cloaks, and so on [33–36].

For example, Vahedpour et al. [37] demonstrated the excitation of higher-order modes in zero-index metamaterial waveguides with two and three defects. Boubakri et al. indicated that a planar metasurface with a reduced tunable size can provide a near-zero refractive index and phase compensation mechanism [38]. Qiu et al. [39] found that zero-refractive-index materials can be made with photonic crystals near a Dirac-like frequency to construct beam splitters and obtain high transmission efficiency. The metamaterial structure designed by Ma et al. [40] achieved high-efficiency broadband transmission with zero refractive index from 10.72 to 11.4 GHz, and low-loss near-zero refraction can be realized by adjusting the electric and magnetic plasma frequencies. Through the previous studies, most of the zero-refractive index metamaterials were mainly concentrated in the single-band characteristics. Wide-band or dual-band zero-index metamaterials should be investigated for wider applications.

In the research about near-zero refractive index metamaterials in terahertz range, Zhang et al. proposed that the near-zero refractive index metamaterials could be realized by properly designing a fishnet metamaterial using full-wave finite-element simulation [41]. Using a periodic array of split ring resonator holes within a terahertz range, Yang et al. numerically and experimentally confirmed zero refractive index at localized waveguide resonant frequency for aluminum film [42]. Khoo et al. proposed an analysis of aligned nematic liquid crystal cells containing core-shell nanospheres to devise a new type of metamaterial with refractive index close to zero [43]. T. Suzuki et al. demonstrated experimentally a zero-refractive-index metasurface with a refractive index of $0.16 + j0.09$, reflectance of 0.7%, and transmittance of 97.3% at 0.505 THz [44]. However, the zero-refractive-index metamaterials studied in the past mainly focused on a single frequency. Here, using a two-sided metal structure, we propose a dual-band near-zero refractive index metamaterial in terahertz band. By optimizing the design of structural parameters, we demonstrate that the effective refractive index can be achieved to be near zero at $0.5 - 1.7$ THz and at $2.7 - 3.4$ THz. The equivalent electromagnetic parameters of the metamaterial structure are extracted using the inversion algorithm. Through monitoring the surface current distribution of the flat structure and the prism simulation of the designed structure, we prove that the designed metamaterial structure has obvious dual-band zero-refractive-index effect in the terahertz band.

2. Effective Parameter Extraction Method

Maxwell proposed the propagation law of time-varying electromagnetic fields and provided the relationship between the relevant physical quantities of electric and magnetic fields in the form of formulas. According to the Maxwell equation, the effective index $n = \sqrt{\varepsilon\mu}$ of a material can be determined by the effective permittivity – dielectric constant ε and effective permeability μ. In order to obtain an effective refractive index close to zero, it is necessary to make the effective dielectric constant or effective permeability close to zero, or both at the same time. According to the effective medium theory [45], the scattering parameter inversion algorithm can be used to inversely calculate the equivalent refractive index n and impedance z of a designed metamaterial. The effective permittivity ε and permeability μ can be obtained as $\varepsilon = n/z$ and $\mu = nz$. When the effective electromagnetic parameters of a designed metamaterial are changed, the specific resonant characteristics of this metamaterial will also change accordingly.

When a metamaterial unit structure is equivalent to a uniform medium, the transmission matrix T of this plane metamaterial can be expressed as follows [46–49]:

$$T = \begin{pmatrix} \cos(nkd) & -(z/k)\sin(nkd) \\ (k/z)\sin(nkd) & \cos(nkd) \end{pmatrix}, \tag{1}$$

where n is the effective refractive index of the material, d is the effective thickness of the material, k is wavenumber, and z is the plane wave impedance. Scattering parameters can be calculated for metamaterials with symmetric structure by transmission matrix; they read

$$S_{12} = S_{21} = \frac{1}{\cos(nkd) - (i/2)\,(z + 1/z)\sin(nkd)}, \qquad S_{11} = S_{22} = \frac{i}{2}\left(\frac{1}{z} - z\right)\sin(nkd). \tag{2}$$

According to the inversion algorithm method for Eq. (2), the effective refractive index and impedance can be calculated; they are

$$n = \frac{1}{kd}\,\cos^{-1}\left[\frac{1}{2S_{21}}(1 - S_{11}^2 + S_{21}^2)\right], \qquad z = \sqrt{\frac{(1 + S_{11})^2 - S_{21}^2}{(1 - S_{11})^2 - S_{21}^2}}. \tag{3}$$

Equations (3) can be directly used to determine the effective refractive index and the impedance of designed metamaterials. The expressions for n and z are complex functions with multiple branches, the interpretation of which can lead to ambiguities in determining the final expressions for permittivity and permeability. In order to address this problem, it has been suggested to use a slab of small thickness and apply the requirement that the permittivity and permeability are continuous functions of frequency [46, 47]. Chen et al. determined the proper branch, using the mathematical continuity of the parameters with special attention to possible discontinuities due to resonances [48]. This method can be called as an iterative one. We also determined the proper branch in the same method. Moreover, D. Smith et al. proposed a modification of the standard S parameter retrieval procedure yielding physically reasonable values for the retrieved electromagnetic parameters [49]. The permittivity ε and permeability μ are then immediately calculated by $\varepsilon = n/z$ and $\mu = nz$ for metamaterials.

3. Dual-Band Zero Refractive Index Metamaterial Design

In this study, we propose a flat plate dual-band electromagnetic metamaterial structure with near-zero refractive index. The unit structure diagram is shown in Fig. 1. The double-faced structure is composed of metal materials and dielectric materials. The substrate of the metamaterial periodic unit structure uses a dielectric polyimide ($\varepsilon = 3.5$). In the terahertz band, the polyimide substrate material is a flexible and transparent material, and its loss is negligible. This material is often used as a substrate for terahertz-band optoelectronic devices. Copper is used for the metal structure. In the simulation, we chose copper because it is cheaper compared to other precious metals during the experimental preparation process. In the terahertz band, the properties of various metal materials are basically the same, so we do not need to use complex models to characterize the properties of materials in the numerical simulation process. The conductivity of $\sigma = 5.8 \cdot 10^7$ s/m was applied for copper in numerical simulations. According to the characteristics of the designed metamaterial, the size of the unit cell should be in the subwavelength range. Furthermore, the grating effect of the size limits the length of the unit cell.

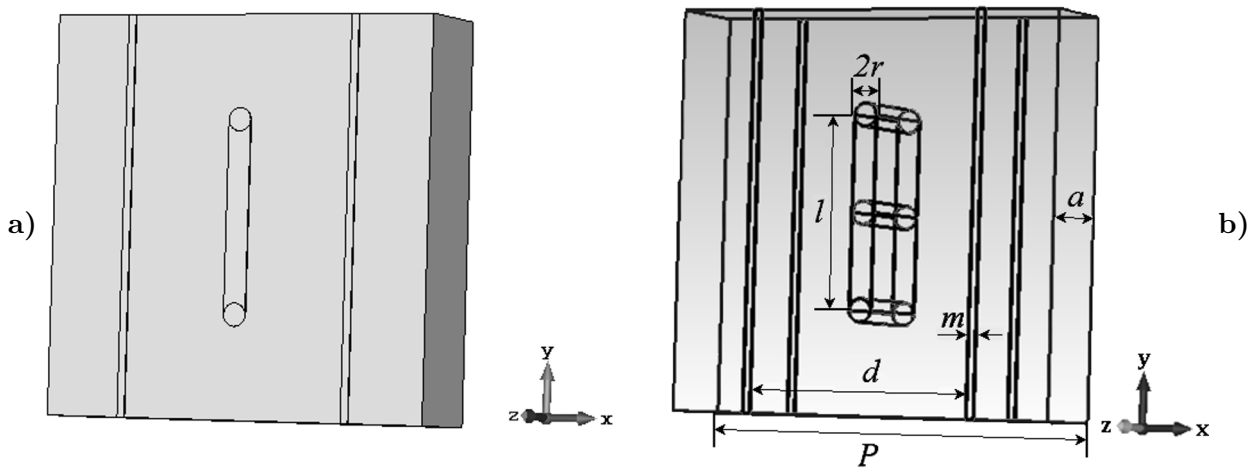

Fig. 1. Unit cell of the designed metamaterial; here, the general view (a) and the transparent view mode (b).

While designing, only zero-order diffraction of periodical units can be allowed to appear, and high-diffraction orders need to be suppressed. The electromagnetic wave at 1 THz frequency corresponds to a wavelength of 300 μm. The initial period size of the unit structure of about 50 μm can be selected in order to match the device in the experiment, and the thickness of polyimide substrate in the terahertz band should be greater than 10 μm. It is known that both the magnetic and electric resonances by double-sided metal structure should be precisely controlled for the transmissive metamaterials. The width and length of the metal lines and the thickness of the base of the unit structure directly affect the resonance characteristics of the electromagnetic field. In addition, combined with the preparation process in the terahertz band, the width of the metal line is generally selected to be about 1 μm. Due to the skin effect of metals in the terahertz band, the thickness of metal structures is generally greater than 0.1 μm.

After the initial structural parameters are determined, we carry out parameter scanning on the basis of these parameters. Parameter-scan optimization-design method is the most basic and simple optimization method. After accurate optimization of design with double-band near-zero refractive index, the geometrical parameters of the element structure can be determined. The period of unit cell is 52 μm and the thickness of substrate is 14 μm. The length of the metal wire is 52 μm, the width is 1 μm, the distance between the two metal wires on the same plane is 31 μm, the radius of the metal via is 1.5 μm, the distance between the adjacent metal vias is 12.5 μm, and the thickness of the metal copper is 0.18 μm. It should be noted that the skin depth of copper of approximately 0.1 μm in the frequency range from 0.5 - 4 THz is revealed [44]. The copper wire in our design is sufficiently thick in comparison with the skin depth of copper. The electromagnetic wave is perpendicularly incident on the surface of the designed metamaterial along the z direction. The electric field vector is along the y direction. The x and y directions are set as periodic boundary conditions (unit cell), and the z direction is set as open boundary conditions. The finite integral method was used to calculate transmission characteristics and electric-field distribution characteristics of the metamaterials designed. In the numerical simulations, the electromagnetic wave characteristics and the near-field distribution of the double-sided metamaterial structure were calculated based on the finite-integral-method software.

When an electromagnetic wave is incident perpendicularly to the surface of the metamaterial, the two pairs of metal plates located in the front and rear planes form two capacitors. The metal plates will

generate LC resonance, and current will flow through the metal plates. The metal copper structure is embedded in the substrate material, and the loop current will be formed to generate an induced magnetic field. The electromagnetic characteristics of the metamaterial structure can be changed by adjusting the electric resonance and the magnetic resonance.

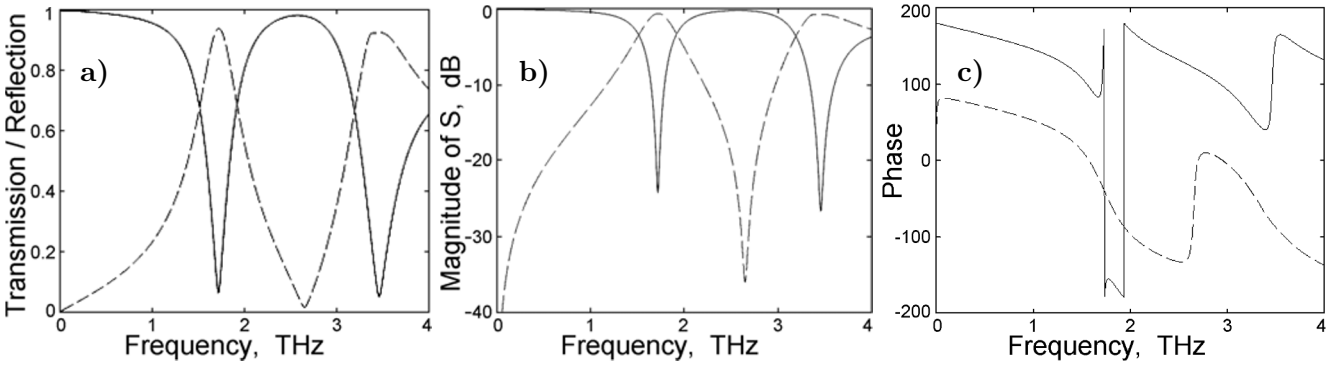

Fig. 2. Transmission/reflection coefficient (a), the amplitude of S parameters in dB form (b), and the transmission phase as a function of frequency (c) with scattering parameter S_{11} (solid curves) and S_{21} (dashed curves).

In Fig. 2, we show the transmission characteristics of the designed metamaterial; here, one can see two high-transmission bands around 1.72 and 3.45 THz (a), the transmission amplitude in dB model (b), and the phase change as a function of frequency (c). We observe that the phase has obvious abrupt change at resonant frequencies.

In view of the effective parameter extraction method, we extract the basic equivalent parameters of designed metamaterial; see Fig. 3. The real and imaginary parts of the effective refractive index n of the metamaterial structure were calculated separately; see Fig. 3 a. One can see that the real part of the refractive index is close to zero at the frequency band about 1.39 – 1.65 THz and 3.10 – 3.26 THz. The smaller imaginary part of the refractive index $\mathrm{Im}\, n$ indicates that the metamaterial has smaller absorption of electromagnetic waves at resonant frequencies. In Fig. 3 b, the real and imaginary parts of the effective permittivity $\mathrm{Re}\, \mu$ and $\mathrm{Im}\, \mu$ at resonant frequencies of 1.66 and 3.34 THz reach the values close to zero. For our metamaterial designed, $\mathrm{Re}\, \mu \sim 1$ and $\mathrm{Im}\, \mu \sim 0$ at resonant frequencies of ∼1.66 and 3.34 THz. Through the extraction of these equivalent parameters, we found that the zero refractive index of double bands can be realized, using the metamaterials constructed with double-sided

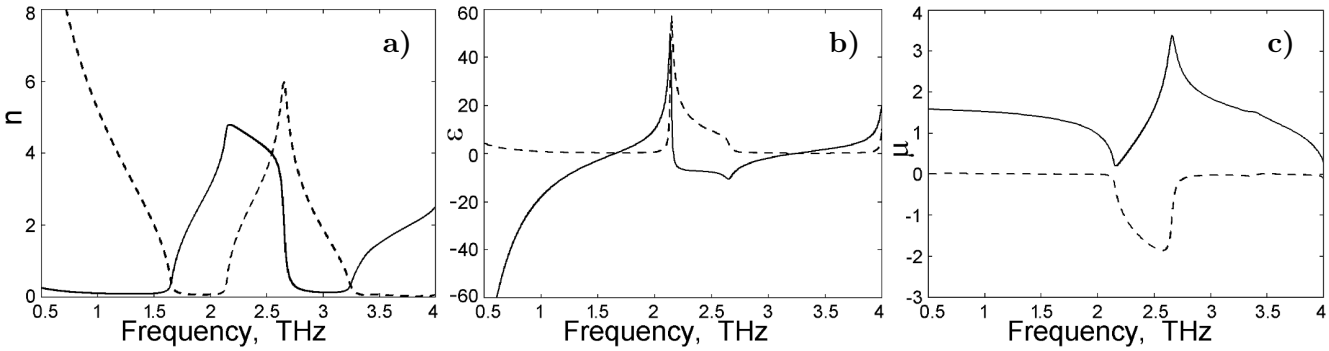

Fig. 3. Retrieved bulk effective refractive index (a), the permittivity (b), and the permeability (c); here, the real parts of these quantities are shown by solid curves and the imaginary parts, by dashed curves.

microstructure. In Fig. 3 c, one can see that the effective permeability demonstrates negative value from ∼2.1 to 2.7 THz. The negativity of the imaginary part of magnetic permeability does not contradict the second law of thermodynamics, nor any other conceivable physical constraints [50]. This phenomenon can be attributed to the energy of a monochromatic electromagnetic field of frequency, which is dissipated into heat at a point inside a spatially uniform medium [51–53].

4. Properties of the Near Field of Zero-Index Metamaterial Designed

In order to verify the zero-refraction characteristics of the designed metamaterial, monitoring of the electromagnetic field and surface current of the metamaterial structure was carried out in [54–57]. The zero-index metamaterial achieved near-zero refractive index at 1.66 and 3.34 THz, and the transmission coefficient exceeded 90%. When an electromagnetic wave enters a zero-index metamaterial from air, only the normal incident wave can penetrate into the metamaterial due to the existence of the critical angle. According to Snell's law, when the electromagnetic wave enters air again, the refraction angle is close to zero, that is, the refracted electromagnetic wave will be perpendicular to the interface. Based on this property, we carried out the verification simulation of the zero refractive-index effect.

As shown in Fig. 4, a single unit structure is arranged in the y axis direction, 15 unit structures are placed in the x axis direction, 15 unit structures are placed in the z axis direction, and the unit structure decreases in a stepped manner. The overall structure presents a triangular shape. In the simulation, the y axis is set as the periodic boundary condition, while the x and z axes directions are set as the open boundary conditions. The waveguide source was used in simulation. When the electromagnetic wave is incident on the metamaterial structure along the z axis direction, the near field distributions are shown in Fig. 5 at 1.66, 2.2, 3.34, and 4.0 THz, respectively. In Fig. 5 a, c, one can see that the final exit direction of the beam is consistent with the normal direction of the slope, indicating that the metamaterial structure can modulate the beam propagation direction. Since the direction of the outgoing wave is perpendicular to the triangular plane, we can obtain the zero refractive index of the designed metamaterial. In Fig. 5 b, d, we see that the beam refraction direction falls into the positive refraction area at 2.2 and 4 THz. The metamaterial structure deviating from the equivalent zero refractive index cannot realize the beam to be perpendicular to the egress interface.

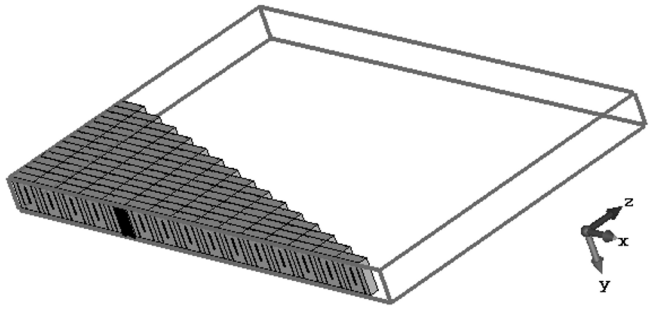

Fig. 4. The electric-field simulation model.

In order to further reveal the zero refractive index of the metamaterial structure designed, we monitor the surface current of the structure at 1.66 THz. In Fig. 6, the current flow direction is shown by the solid arrow, the electromagnetic wave is normally incident on the surface of the metamaterial structure along the z axis, and the electric field vector is along the y axis. We found that the current directions on the metal sheet located in the front and back planes are opposite, and the metal wire produces LC resonance. The loop current formed by the metal copper structure will generate an induced magnetic field; its direction is opposite to the direction of the incident magnetic field.

To study the influence of the geometric parameters of the flat double-band metamaterial structure on the refractive index, we change the length of the middle metal wire l, the thickness of the unit structure

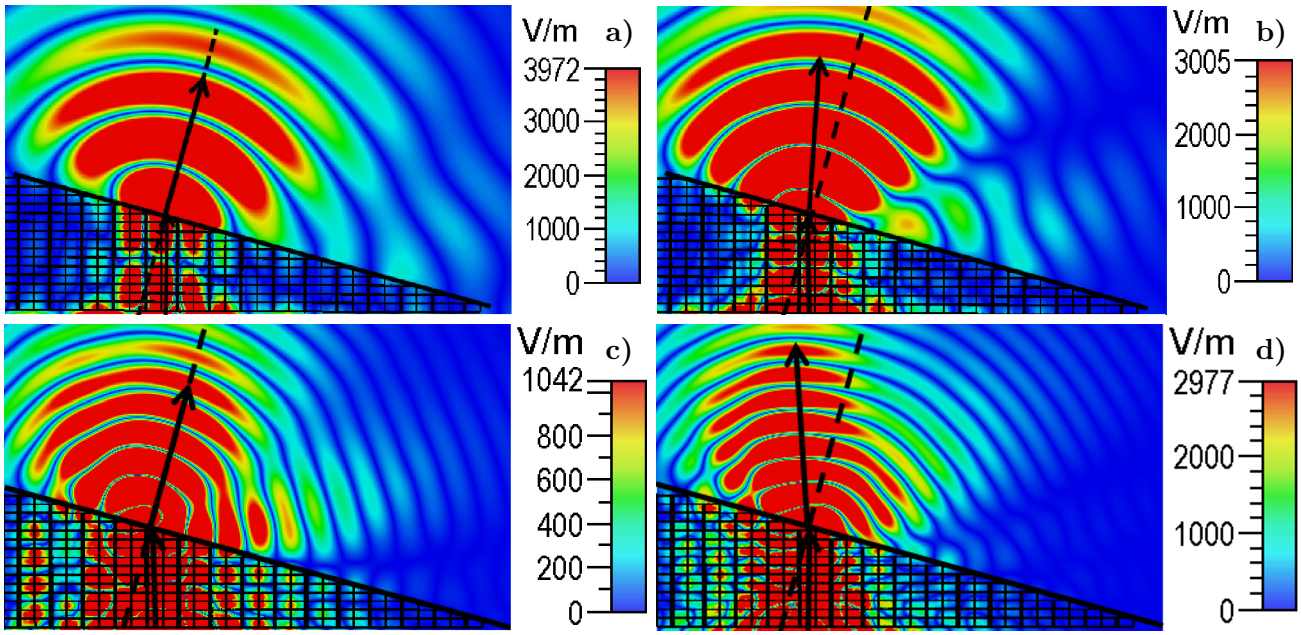

Fig. 5. The electric field distribution in the designed metamaterial at 1.66 THz (a), 2.2 THz (b), 3.34 THz (c), and 4 THz (d).

a, the distance d of the two metal wires on the same plane, and the radius r of the metal.

The change in the real part of equivalent refractive index $\mathrm{Re}\, n$ of the metamaterial structure is shown in Fig. 7; here, the period of unit cell is 52 μm and the thickness of substrate is 14 μm. The width of two metal wires is 1 μm, and its length is equal to the period of the unit structure. The width of the wire at the center of the unit structure is equal to the diameter of the metal vias. The distance between the two metal wires on the same plane is 31 μm. The thickness of the metal copper is 0.18 μm. Keeping the radius of the metal via $r = 1.5$ μm embedded in the material, the influence of the length l of the middle metal wire on the refractive index is shown in Fig. 7 a. With increase in the length of the metal wire, the refractive index curve is red-shifted to the resonant region. Keeping the length $l = 25$ μm of the middle metal wire unchanged, as the radius of the metal via increases (Fig. 7 b), the refraction index of the metamaterial is red-shifted at 1.5 – 2 THz and blue-shifted at 2 – 4 THz and $\Delta f_1 \approx \Delta f_2$. At the length $l = 25$ μm of the middle metal wire and the radius $r = 1.5$ μm of the metal via, we see in Fig. 7 c that as the thickness a of the cell structure increases, the refractive

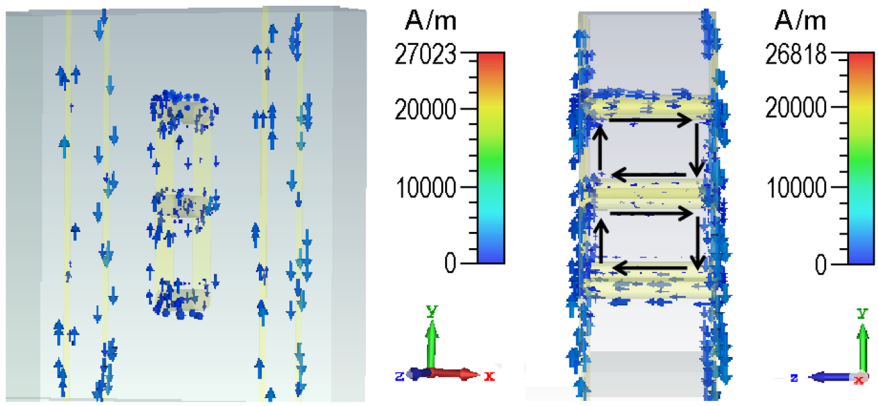

Fig. 6. Surface current density distribution on the metamaterial structure at 1.66 THz; here, the front view is shown on the left and the lateral plane, on the right.

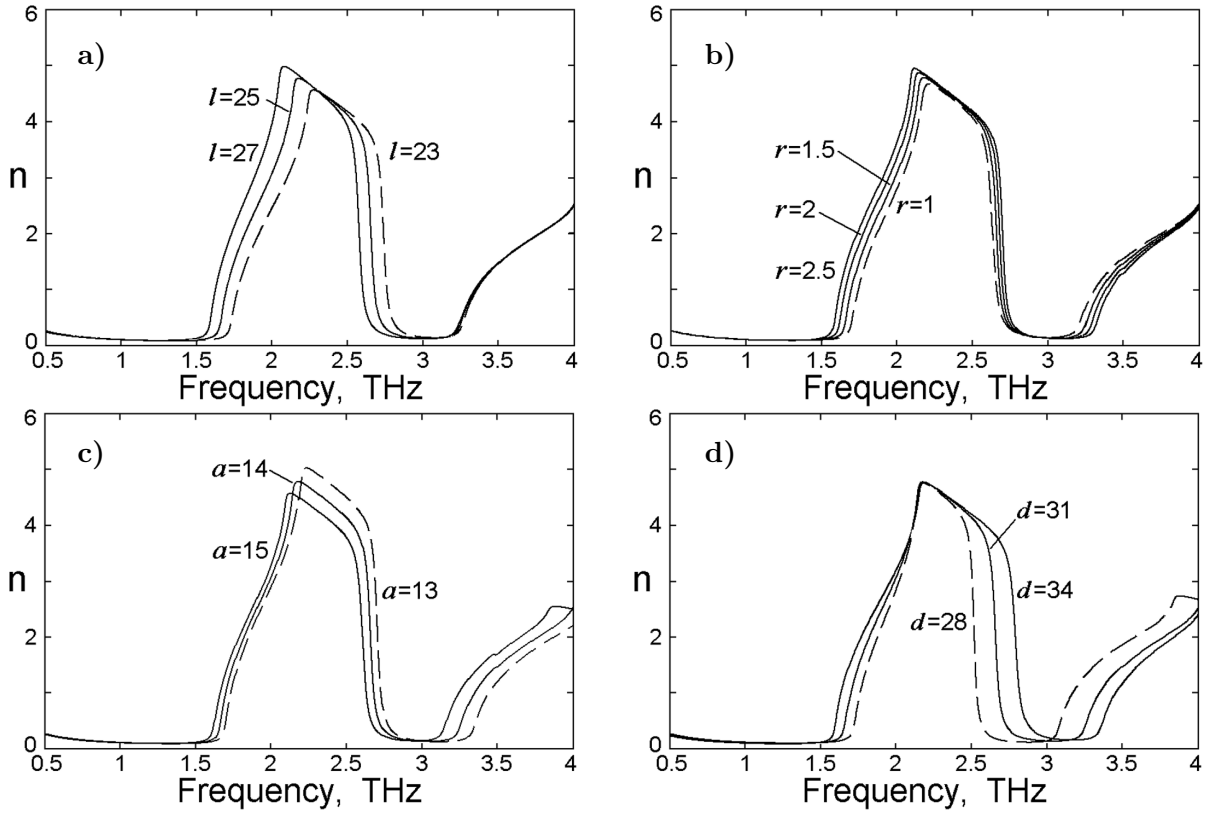

Fig. 7. Influence of structural parameters on the refractive index; namely, the effect of the length l of the intermediate wire (a), the effect of the metal pore radius r (b), the influence of the element structure thickness a (c), and the effect of the distance d between two wires in the same plane (d).

index is also red-shifted. In Fig. 7 d, with increase in the distance d between two metal lines on the same plane, high refractive-index bandwidth is widened at the resonant region. Zero refractive index region around 3.0 THz is red-shifted with increasing d.

There are two pairs of metal wires in the structure, and the current densities of the metal wires on the front and back surfaces are approximately equal at 1.66 THz. In Fig. 8, we show dependences of the real part of the refractive index and transmission coefficient on the metal line width m; here, the unit cell period is 52 μm and the substrate thickness is 14 μm. Also, the wire width at the center of the unit structure is equal to the diameter of the metal vias, the distance between the two metal wires on the same plane is 31 μm, and the thickness of the metal copper is 0.18 μm. In addition, the radius of the metal via $r = 1.5$ μm and the length $l = 25$ μm of the middle metal wire are maintained. As the width of the metal line increases, the value of the equivalent refractive index drops significantly at $0.5 - 1.7$ THz. We obtained that increasing the width of the metal line can make the structure's refractive index closer to the ideal value of zero. As shown in Fig. 8 b, the transmission coefficient on the width of the metal line shows a clear blue shift at the second transmission peak. In the frequency band near zero refractive index, the transmission passband is the widest and the transmission coefficient of the terahertz wave can reach more than 90%.

Assuming that the ratio between the widths of the metal line on the back surface and the front surface

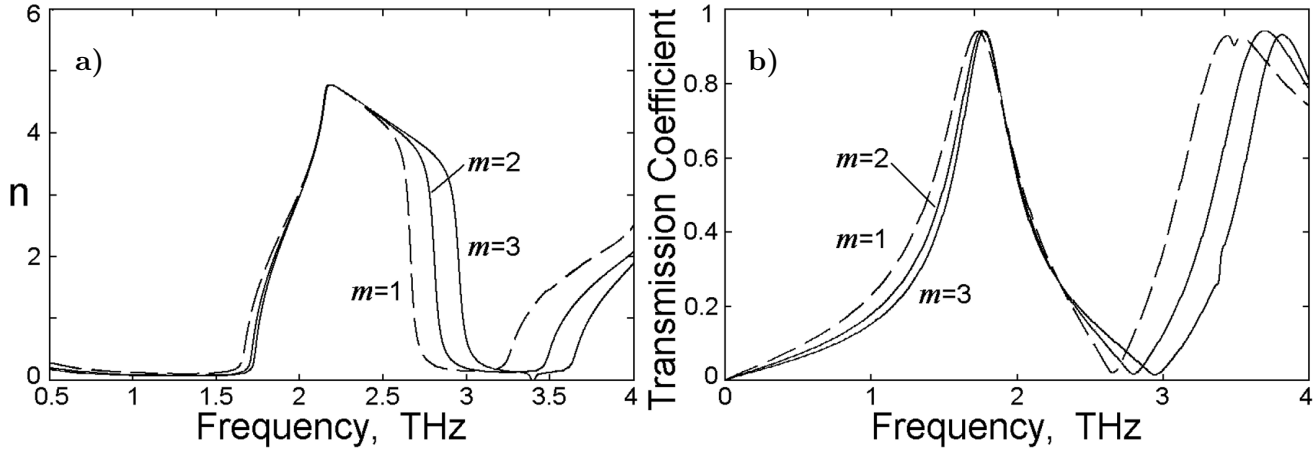

Fig. 8. Influence of the wire width m on the effective refractive index (a) and the transmission coefficient (b).

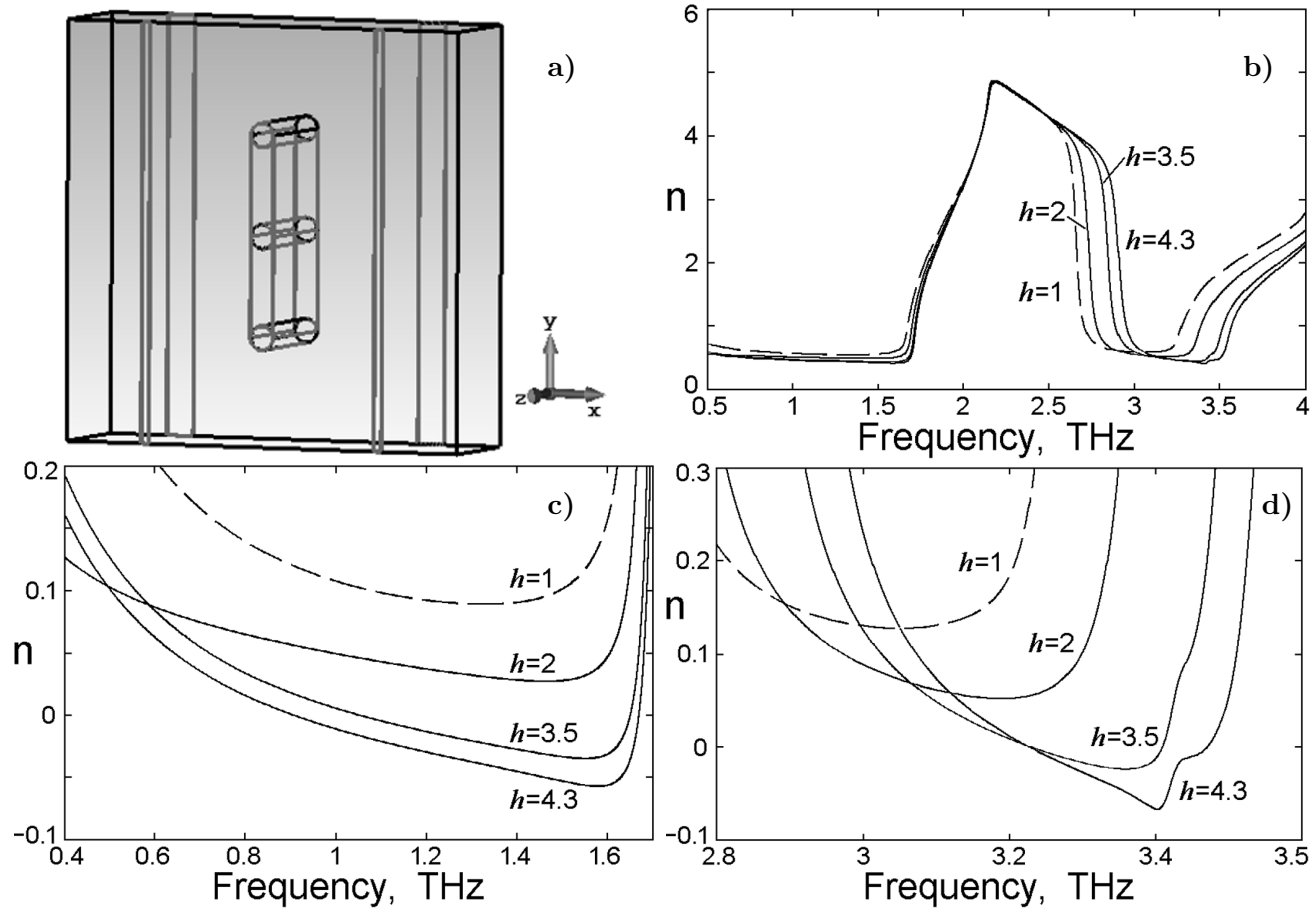

Fig. 9. A transparent view of the schematic (a), the real part of the effective index with different h (b), enlarged equivalent refractive index view at the first resonant region (c), and enlarged equivalent refractive index view at the second resonant region (d).

is h, an asymmetry model of metamaterial can be established to study the effect of the width of the metal line on the refractive index of the structure. The geometric meaning of the parameter h is the ratio of the metal linewidths of the front and back surfaces. The width of two metal wires on the front surface is 1 μm, and its length is equal to the period of the unit structure, i.e., if the ratio $h = 2$, the wire width on the back surface is 2 μm. We consider the change in this ratio mainly to study the change in effective parameters of metamaterials due to the asymmetry of double-sided structure. Here, the unit cell period is 52 μm and the substrate thickness is 14 μm. The wire width at the center of the unit structure is equal to the diameter of the metal vias. The distance between the two metal wires on the same plane is 31 μm and the thickness of the metal copper is 0.18 μm. The radius of the metal via $r = 1.5$ μm and the length $l = 25$ μm of the middle metal wire are maintained. The width of two metal wires on the front surface is 1 μm, and its length is equal to the period of the unit structure. The real part of the effective refractive index with different ratio $h = 1$, 2, 3.5, and 4.3, respectively, is revealed as shown in Fig. 9, with the transparent view of the schematic shown in Fig. 9 a and the effective refractive index with different ratio h, in Fig. 9 b. As the ratio h increases, the second zero refractive index band at about 3.0 THz demonstrates the blue shift while the first zero refractive index band remains essentially unchanged. In the zero refractive index region, the enlarged equivalent index view is shown in Fig. 9 c, d. By increasing the metal wire width on the rear surface, one can substantially reduce the refractive indices of the two frequency bands, and the ideal value of zero refractive index appears near 1.66 and 3.34 THz. One can conclude that the h parameter effectively reduces the value of the equivalent zero refractive index of the metamaterial structure and widens the frequency band of near zero refractive index.

As the parameter h increases, the transmission peak of the metamaterial also shifts, and as shown in Fig. 10, the first transmission peak decreases slightly, but the transmission passband decreases significantly. The second transmission peak has a significantly lower peak value, and the transmission peak shows the blue shift. Therefore, on the premise of ensuring a large transmission coefficient and zero refractive index, the optimum value of parameter h is determined to be 3.5. At 1.66 and 3.34 THz, with $h = 3.5$, the transmission coefficient at both frequencies still reaches 82%, and the refractive index value becomes smaller; see Figs. 9 and 10. Thus, a larger near-zero refractive index terahertz band is obtained.

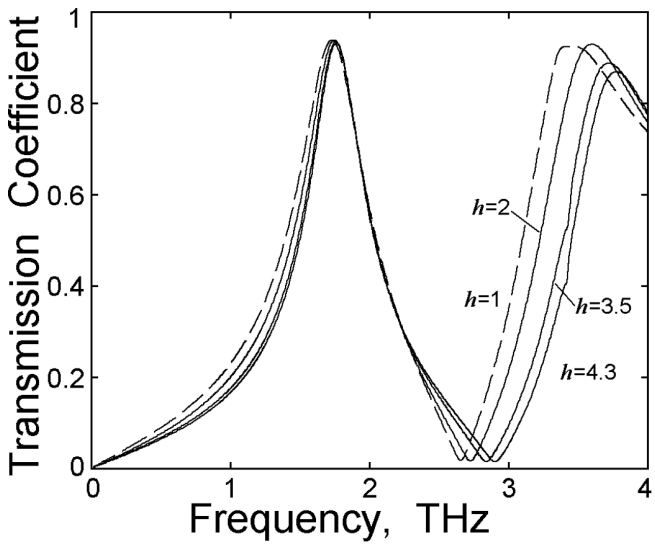

Fig. 10. Transmission coefficient with different ratio h.

The structural parameters of the double-sided metamaterial can effectively control the electromagnetic characteristics. The electric resonance properties of metamaterials are based on the interaction of propagating terahertz waves with metal wires. The electric resonant properties of the metamaterial structure are characterized by the effective permittivity. The magnetic resonance properties of metamaterials are derived from the metal structure of the front and rear surfaces of the metamaterials. The relative permeability is used to demonstrate the magnetic resonance properties of metamaterials. The equivalent circuit can be adequately applied to explain the electric and magnetic properties of metamaterials. The electric resonance properties in the metamaterial are mainly determined by the inductance component

of metal wires and the capacitance component at a gap between metal wires in a series circuit. The series circuit behaves as a resonance circuit with the inductance and capacitance components at a resonant frequency [44]. The resonance of the series circuit represents the electric resonances. The magnetic resonance in the metamaterial is mainly determined by the inductance and capacitance components of the metal lines on the front and back surfaces. Therefore, the capacitance and inductance of the equivalent circuit can be changed by changing the structural parameters of the metamaterial. Changes in the capacitance and inductance of the equivalent circuit will change the frequency of the electric resonance and magnetic resonance. The red/blue shift of the dispersion of the effective refractive index can be deduced by changing the electric resonance and magnetic resonance of metamaterial with different geometric parameters.

5. Summary

In summary, the metamaterial structure designed achieves the effect of zero refractive index under the condition of normal incidence at terahertz range. In the 0.5 – 1.7 THz and 2.7 – 3.4 THz bands, the equivalent refractive index of the metamaterial structure is close to zero. We analyzed the occurrence of zero refractive index characteristics by monitoring the surface current density distribution of the structure, and the simulation results prove that, at 1.66 and 3.34 THz, the structure has zero refractive index effect and the transmission efficiency reaches more than 90%. We found that the length of the metal line, the thickness of the cell structure, the distance between the two metal lines, the radius of the metal via, and the width of the metal line can affect the characteristics of the effective refractive index. We further investigated the effect of the asymmetry on the effective index of metamaterial and showed that the asymmetry is characterized by the ratio of the width of the front metal line to the width of the back metal line in the double-sided structure. We found that the asymmetry can effectively reduce the value of the equivalent zero refractive index of the metamaterial structure and widen the frequency band of near zero refractive index. The designed metamaterial is simple and convenient to be prepared, and can be applied to the integrated antennas and other photoelectric devices.

Acknowledgments

This work was supported by the Natural Science Foundation of Zhejiang Province under Grants Nos. LZ21A040003 and LY20F050007 and the National Natural Science Foundation of China (NSFC) under Grants Nos. 61904169, 61904168, and 61875179.

References

1. X. He and H. Lu, *Nanotechnology*, **25**, 325201 (2014).
2. X. He, *Carbon*, **82**, 229(2015).
3. H. Guan, H. Chen, J. Wu, et al., *Opt. Lett.*, **39**, 170 (2014).
4. X. He, X. Zhong, F. Lin, et al., *Opt. Mater. Express*, **6**, 331 (2016).
5. X. Luo, Z. Tan, C. Wang, et al., *Chinese Opt. Lett.*, **17**, 093101 (2019).
6. W. Liang, Z. Li, Y. Wang, et al., *Photon. Res.*, **7**, 318 (2019).
7. T. Hou, Y. An, Q. Chang, et al., *High Power Laser Sci. Eng.*, **7**, e59 (2019).
8. S. Teng, Q. Zhang, H. Wang, et al., *Photon. Res.*, **7**, 246 (2019).

9. M. Akram, G. Ding, K. Chen, et al., *Adv. Mater.*, **32**, 1907308 (2020).
10. M. Akram, M. Mehmood, X. Bai, et al., *Adv. Opt. Mater.*, **7**, 1801628 (2019).
11. W. Zhu, M. Jiang, H. Guan, et al., *Photon. Res.*, **5**, 684 (2017).
12. H. Wang, L. Liu, C. Zhou, et al., *Nanophotonics*, **8**, 317 (2019).
13. Q. Zhang, H. Wang, L. Liu, et al., *Opt. Express*, **26**, 24145(2018).
14. H. Wang, L. Liu, C. Liu, et al., *New J. Phys.*, **20**, 033024 (2018) .
15. Z. Zhang, G. Chen, M. Yang, et al., *Nanophotonics*, **9**, 2387 (2019).
16. X. Jing, X. Gui, P. Zhou, et al., *J. Lightw. Technol.*, **36**, 2322 (2018).
17. R. Xia, X. F. Jing, X. C. Gui, et al., *Opt. Mater. Express*, **7**, 977 (2017).
18. J. Zhao, X. Jing, W. Wang, et al., *Opt. Laser Technol.*, **95**, 56 (2017).
19. W. Wang, X. Jing, J. Zhao, et al., *Opt. Appl.*, **47**, 183 (2017).
20. L. Chen, X. Jing, Y. Tian, et al., *J. Laser Appl.*, **27**, 022001 (2015).
21. L. Chen, X. Jing, L. Wang, et al., *Opt. Laser Technol.*, **62**, 95 (2014).
22. J. Mian, H. Zhu, D. Zhu, et al., *Optoelectron. Adv. Mat.*, **11**, 148 (2017).
23. Y. Wu, S. Jin, X. Jing, et al., *Opt. Eng.*, **51**, 128001 (2012).
24. L. Jiang, B. Fang, Z. Yan, et al., *Microw. Opt. Technol. Lett.*, **62**, 6 (2020).
25. X. Jing, Y. Ke. Y. Tian, et al., *IEEE Access.*, **8**, 164795 (2020).
26. X. Jing, Y. Xu, H. Gan, et al., *IEEE Access.*, **7**, 144945, (2019).
27. B. Fang, C. Li, Y. Peng, et al., *Microw. Opt. Technol. Lett.*, **61**, 1634 (2019).
28. B. Fang, Z. Cai, Y. Peng, et al., *J. Electromagnet. Waves*, **33**, 1375 (2019).
29. B. Fang, B. Li, Y. Peng, et al., *Microw. Opt. Technol. Lett.*, **61**, 2385 (2019).
30. X. Jing, S. Jin, Y. Tian, et al., *Opt. Laser Technol.*, **48**, 160 (2013).
31. Y. Fu, L. Xu, Z. Hang, et al., *Appl. Phys. Lett.*, **104**, 193509 (2014).
32. C. Zhang, C. Chan, and X. Hu, *Sci. Rep.*, **4**, 6979 (2014).
33. X. Jia and X. Wang, *Optik*, **182**, 464 (2019).
34. A. Evangelos, M. Amanollahi, M. Zamani, et al., *Opt. Mater.*, **99**, 109539 (2019).
35. E. Mohammadi, K. L. Tsakmakidis, F. Sohrabi, et al., *Microw. Opt. Technol. Lett.*, **58**, 233 (2019).
36. M. Bhaskar, E. Johari, Z. Akhter, et al., *Microw. Opt. Technol. Lett.*, **58**, 233 (2015).
37. A. Roghayyeh and M. Z. B. Vahedpour, *Opt. Commun.*, **403**, 170 (2017).
38. A. Boubakri, F. Choubeni, T. H. Vuong, et al., *Opt. Mater.*, **69**, 432 (2017).
39. P. Qiu, W. Qiu, Z. Lin, et al., *Sci. Rep.*, **7**, 9588 (2017).
40. J. W. Ma, X. Q. Zhu, S. Bi, et al., *Opt. Commun.*, **446**, 113 (2019).
41. Q. L. Zhang, L. M. Si, Y. Huang, et al., *AIP Adv.*, **4**, 037103 (2014).
42. J. K. Yang, C. Kang, I. Sohn, et al., *Opt. Express*, **18**, 25371 (2010).
43. I. C. Khoo, D. H. Werner, X. Liang, et al., *Opt. Lett.*, **31**, 2592 (2006).
44. T. Suzuki and H. Asada, *Opt. Express*, **28**, 21509 (2020).
45. L. Jiang, B. Fang, Z. G. Yan, et al., *Opt. Laser Technol.*, **123**, 105949 (2020).
46. P. Markoš and C. M. Soukoulis, *Opt. Express B*, **11**, 649 (2003).
47. D. R. Smith, S. Schultz, P. Markoš, et al., *Phys. Rev. B*, **65**, 195104 (2002).
48. X. Chen, T. M. Grzegorczyk, B. I. Wu, et al., *Phys. Rev. E*, **70**, 016608 (2004).
49. D. R. Smith, D. C. Vier, T. Koschny, et al., *Phys. Rev. E*, **71**, 036617 (2005).
50. V. A. Markel, *Phys. Rev. E*, **78**, 026608 (2008).
51. R. A. Depine and A. Lakhtakia, *Phys. Rev. E*, **70**, 048601 (2004).
52. A. L. Efros, *Phys. Rev. E*, **70**, 048602 (2004).
53. T. Koschny, P. Markos, D. R. Smith, et al., *Phys. Rev. E*, **68**, 065602 (2003).
54. L. Koirala, C. Park, S. Lee, et al., *Chinese Opt. Lett.*, **17**, 082301 (2019).
55. M. Huault, D. D. Luis, J. Apinaniz, et al., *High Power Laser Sci. Eng.*, **7**, e60 (2019).
56. B. Du, H. B. Cai, W. S. Zhang, et al., *High Power Laser Sci. Eng.*, **7**, e40 (2019).
57. S. Rubin and Y. Fainman, *Adv. Photon.*, **1**, 066003 (2019).